Control& Implementation of Fuzzy Based DFIG Wind Power Generators in Unbalanced Micro grids

Dr.RAMACHANDRA C G

[1]PG Student, Dept. of EEE, Sri Padmavathi Mahila University, Tirupati .
[2]Ph.D &Assistant Professor, Dept. of EEE, Sri Padmavathi Mahila University, Tirupati .

Abstract—This work presents a proposed power system with a diesel generator (DG), wind energy conversion system and solar photo voltaic (PV) system. The proposed power system with its control techniques, regulates the loading of DG to achieve a low specific fuel consumption with the help of wind energy conversion systems (WECS) and SPV system. The doubly fed induction generator (DFIG) is used in WECS system. The WECS system consists of two voltage source converters (VSCs) for the system control. One converter is FUZZY based RSC Control Strategy(RSC), which helps in achieving maximum power point tracking of the wind turbine. Another one is the generator side converter (GSC), which helps in regulating DG generation while maintaining WECS generator as well as Diesel generator currents balanced, unbalanced and harmonics within the requirement of the IEEE-519 standard at different load conditions. The system envisages energy storage by connecting a battery bank at the DC bus of DFIG. The battery bank provides buffer storage. To increase optimal operation, solar PV system with MPPT technique also integrated with DG system, and SPV system with MPPT algorithm maintain DC link voltage. The proposed power system is modelled using MATLAB Sim-power-system tool box and proposed system performance results are presented under variation of linear loads, nonlinear loads, unbalanced loads.

Index Terms—
Wind Turbine, doubly fed induction generator (DFIG), diesel generator, solar photovoltaic arra y, bidirectional buck/boost DC-DC converter, battery energy storage, power qu ality.

1. INTRODUCTION

Diesel generators (DGs) are very popular for the d ecentralized power generation as well as backup po wer in the urban housing society for the following reasons [1]-[3].

- DGs are portable and dispatchable.
- They are of lower capital cost.
- DGs maintenance is easier.
- They have higher conversion efficiency as compared to other sources of energy resu lting in low specific greenhouse gas emiss ion.

For the above reasons, they are widely used for the power distribution of islands, commercial and mili tary ships etc [4]. However, DGs suffer from the hi gher running cost along with noise and air pollutio n. The running cost is dependent on amount of fuel consumption based on the power generation. This cost is minimized b y installing renewable energy (RE) sources such as wind, solar and biomass etc. Moreover, RE based power sources are pollution free and abundant in n ature. Among RE sources, wind and solar are consi dered to be more popular because of their reduced cost and technological advancements [5], [6]. Win d turbines are mainly categorized as fixed speed an d variable speed type. Fixed speed wind turbines h ave been used earlier due to their simple operating features. However, they suffer with more power lo ss. Variable speed wind turbines with doubly fed i nduction generator (DFIG), are dominantly used fo r wind energy extraction due to its advantages such as reduced converter rating, less acoustic noise, hi ghly energy efficient and low power loss [7]. Subst antial literature on DFIG based wind energy conversion system (WECS) both in standalone [8] and grid connected modes, is available [9]-[11]. In [8], the authors have presented DFIG base d WECS operating in standalone with a battery ene rgy storage (BES) connected directly at the DC lin k. Moreover, the comparative performance with an d without BES is discussed. In [9], the authors hav e described an extended active power theory for eff ective operation of wind turbine coupled DFIG bot h in balanced and unbalanced grid conditions. Mor eover, the DFIG is controlled with only rotor side converter (RSC). Therefore, the topology suffers fr om the power quality issues especially during harm onic loads. Liu *et al.* [10] have investigated the infl uence of phase locked loop parameters and grid str ength on the stability of DFIG wind farm in grid connect ed mode. However, an experimental validation has

not been performed. In [11], the authors have discu ssed a synchronization control method for smooth connection of DFIG to the grid. Moreover, it has b een implemented on a modified IEEE 39 bus system using real time simulation platform. However, hardware realization has not been done. In other side, there has been increasing power gene ration through solar photovoltaic (PV) array world wide. The solar energy conversion system (SECS) can be single stage or double stage. Some of the lit erature regarding solar PV system is reported in [1 2], [13]. Shah *et al*. [12] have demonstrated the sin gle stage SECS connected to the utility grid. More over, a fundamental current extraction technique b ased on second-order generalized integrator with frequency-locked loop has been implemented for voltage sour ce converter (VSC). In [13], the authors have prese nted the double stage SECS interacting to the grid. In addition, an adaptive algorithm of fast zero attra cting normalized least mean fourth has been imple mented for VSC to improve the power quality issu es.

The operation of WECS and SECS separa tely, is not economical and reliable because of thei r intermittency. Therefore, the integration of both wind and solar sources, improves reliability of pow er generation [14], [15]. Morshed *et al.* [14] have p resented wind-PV system with fault ride through capabilities. In it s topology, the solar PV array is connected at the DC link of DFIG based WECS through a boost co nverter and a DC-DC converter. However, it increases the switching losses and cost, because of additional DC-DC converter along with grid side converter. In [1 5], the authors have demonstrated the wind-solar PV system with BES in standalone mode. In i ts configuration, the solar PV array is connected at the DC link of wind turbine driven DFIG through a boost converter. However, the current through BE S is not controlled, because it is directly connected at the DC link. Further, the microgrids based on DG, wind and solar sources have been develop ed and reported in the literature [16]-[18]. In [16], the authors have discussed the capaci ty plFuzzying of BES for a microgrid based on wind, solar and diesel sources that are located i n island. However, optimal fuel operation of DG h as not been discussed. In [17], the authors have de monstrated a wind-diesel microgrid for fuel efficient zone with BES. However, the BES current is not controlled due to its direct connection at the DC link. Moreover, the chances of getting away from fuel efficient zone is more due to connection of only one RE source. Ve nkatraman *et al.* [18] have presented a wind-solar-diesel microgrid with BES for certain remote area. However, the optimal operation of DG has been ig nored while developing the source and load control lers. In any microgrid, the BES plays vital role duri ng the mismatch of generation and demand. Moreo ver, it helps in extraction of maximum power both from wind and solar, especially when the generatio n is more than the demand. There are many maxim um power point tracking (MPPT) techniques discu ssed in the literature, both for wind and solar to ext ract maximum power corresponding to particular w ind speed and insolation, respectively [12], [13], [1 5], [19], [20].

This work presents a microgrid based on wind turbine driven DFIG, DG and solar PV ar ray with BES, in order to minimize the fuel consu mption of DG. In this, the DG is designed to delive r the base load requirement of a particular househo ld locality. The main contributions of this study are on the control aspects of the scheme, which are as follows.

- A novel generalized concept is used to co mpute the reference DG power output for the DG to remain operating in optimal fue l consumption mode.
- The load side converter control (LSC) is d esigned to control DG along with the pow er quality issues such as load unbalance c ompensation, harmonics compensation an d reactive power compensation.
- The RSC control is designed to extract ma ximum power from the wind turbine.
- The BES is connected to the common DC bus of back-back connected VSCs through a bidirectio nal buck/boost DC-DC converter. It aims to provide path for excess stator power of DFIG. Moreover, a solar PV array is directly connected at D C bus.
- The bidirectional buck/boost DC-DC converter control is designed in a way to extract maximum power from the solar PV array and to control the current throu gh BES.
- A modified perturb and observe (P&O) M PPT algorithm is presented to obtain maxi mum power from a solar PV array.
- This microgrid configuration is implement ed with minimum number of converters, t hereby reducing the total system cost and switching losses.
- The DFIG stator currents and DG currents are maintained balanced and sinusoidal, a s per the IEEE 519 standard.

The wind-diesel-solar microgrid with BES is modelled and simulate d using SimPowerSystems tool box of MATLAB. The system performance is analysed for variable w ind speeds, variable insolation, effect on buck boost converter at varying loads and unba lanced nonlinear load connected at point of commo

n coupling (PCC). To validate the microgrid operat ion, tests are performed
on a developed prototype in the laboratory.

II. CONFIGURATION OFMICROGRID

The schematic configuration of the micro grid is depicted in Fig.
1. It consists of wind turbine, DFIG, DG, solar PV array, BES, bidirectional buck/boost DC-DC converter, RSC, LSC, interfacing inductors, Δ/Y transformer, linear and nonlinear loads, circuit b reakers (CB1 &
CB2), DC link capacitor and ripple filters etc. Thi s microgrid is designed to deliver a peak load of
7.5 kW for a particular locality. The wind turbine generator and solar PV array, are designed to deliv er a power of
7.5 kW each. In this scheme, the solar PV array is directly connected to DC link, whereas BES is co nnected through bidirectional buck/boost DC-DC converter. The DG is comprising of a synchron ous generator of
4 pole, internal combustion engine of
4 stroke reciprocating type along with automatic v oltage regulator (AVR). A
7.5 kVA DG is selected in line with rated capacity of the wind turbine generator. The design of a win d turbine generator, solar PV array, DG, BES and other components, is carried out based
on the literature reported in [12], [15], [17]. More over, the design parameters of microgrid, are given in Appendices.

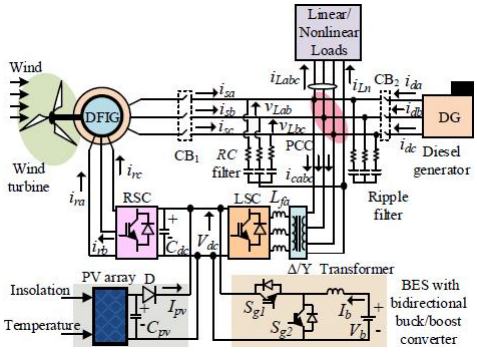

Fig. 1. DFIG based microgrid.

III Developing Control for the New Scheme.

The schematic configuration of the micro grid is depicted in Fig.
4.8. It consists of wind turbine, DFIG, DG, solar P V array, BES, bidirectional buck/boost DC-DC converter, RSC, LSC, interfacing inductors, Δ/Y transformer, linear and nonlinear loads, circuit b reakers (CB1 &
CB2), DC link capacitor and ripple filters etc. Thi s microgrid is designed to deliver a peak load of
7.5 kW for a particular locality. The wind turbine generator and solar PV array, are designed to deliv er a power of
7.5 kW each. In this scheme, the solar PV array is directly connected to DC link, whereas BES is co nnected through bidirectional buck/boost DC-DC converter. The DG is comprising of a synchron ous generator of
4 pole, internal combustion engine of
4 stroke reciprocating type along with automatic v oltage regulator (AVR). A
7.5 kVA DG is selected in line with rated capacity of the wind turbine generator. The design of a win d turbine generator, solar PV array, DG, BES and other components, is carried out based
on the literature reported in [12], [15], [17]. More over, the design parameters of microgrid, are given in Appendices.

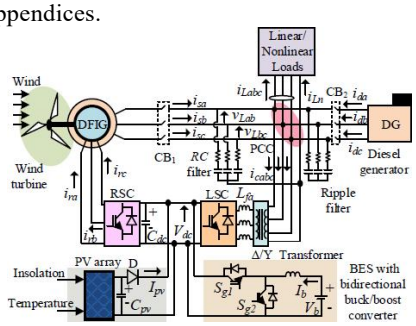

Fig.2. DFIG based microgrid.

The complete description of control algorithms of RSC and LSC, MPPT algorithm of solar PV array, bidirectional buck/boost DC-DC converter, are given in following subsections.

A. Control Algorithm for RSC

The control algorithm of RSC, is depicted in Fig.
2. The RSC is used to supply the reactive power r equirement of DFIG

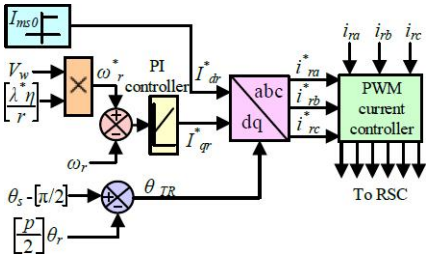

Fig.3. RSC control algorithm.

and also, to regulate the speed for achieving MPPT from the wind turbine. The field-oriented vector control (FOVC) is used for RSC to generate the switching pulses, as shown in Fig.
4.9. In FOVC, direct axis and quadrature axis co mponents of rotor currents (*I*dr*, *I*qr*) represent re active and active components, respectively. The *I* dr* is corresponding to no load magnetizing current (*Ims0*) of DFIG, which is computed as [21],

$$I_{ms0} = \frac{\sqrt{2}V_L}{\sqrt{3}X_m} \quad (1)$$

where *Xm* denotes the magnetizing reactance of the machine and *VL* is the line voltage at the machine terminals.
The *I*qr* is estimated by passing the speed error th rough proportional and integral (PI) controller as d epicted in Fig. 4.9 and it is derived as,

$$I^*_{qr(k)} = I^*_{qr(k-1)} + K_{p\omega}\left(\omega_{err(k)} - \omega_{err(k-1)}\right) + K_{i\omega}\omega_{err(k)} \quad (2)$$

where *Kpω* and *Kiω* represent proportional and int egral constants of PI speed controller, respectively.
The *ωerr(k)* and *ωerr(k-1)* denote speed error at *k*th and (*k*-1)th instants, respectively.
The *ωerr(k)*, is obtained as,

$$\omega_{err(k)} = \omega^*_{r(k)} - \omega_{r(k)} \quad (3)$$

where *ω*r(k)* and *ωr(k)* denote the reference and s ensed rotor speed of DFIG at kth instant, respectiv ely.
The reference rotor speed is obtained from the tip s peed ratio MPPT control [19] as,

$$\omega^*_r = \eta\lambda^* V_w / r \quad (4)$$

where *Vw* λ∗, *η*, and *r* represent wind speed, optimal tip speed ratio , gear ratio and radius of wind turbine, respectively .
The rotor transformation angle (*TR*) is computed as,

$$\theta_{TR} = \left(\theta_s - \frac{\pi}{2}\right) - \left(p/2\right)\theta_r \quad (5)$$

where *s* is obtained from phase locked loop and *r* is computed from the sensed rotor speed as,

$$\theta_r = \int_0^t (\omega_r)dt \quad (6)$$

Finally, reference rotor currents (*i*ra*, *i*rb* and *i*rc*) are derived from *I*qr* and *I*dr* using an angl e of transformation *θTR*, as depicted in Fig. 2. These reference currents along with sensed roto r currents (*ira*, *irb* and *irc*), are applied to pulse wi dth modulation (PWM) controller to produce RSC gating signals.

B. Control Algorithm for LSC

The LSC control algorithm is depicted in Fig. 3. The LSC is controlled to achieve the following objectives.

- It maintains the DG and DFIG stator curre nts sinusoidal and balanced.
- It regulates the DG power within the rang e of *PDmin* to *PDmax* to achieve optimal fuel consumption. Where *PDmin* and *PD max* refer to minimum and maximum DG power output in pu for optimal fuel consu mption.

A modified indirect vector control based on voltage-oriented reference frame, is used to generate the reference currents as shown in Fig. 3. In this, both DG and DFIG stator currents are a dded and controlled to extract maximum power fro m the DFIG and to regulate the DG power within t he range for optimal fuel consumption. The d-axis component of LSC is obtained as,

$$I^*_{dg} = I^*_{dd} + I^*_{dw} \quad (7)$$

where *I*dd*, *I*dw* denote the d-component current of DG and DFIG, respectively.
It is noted that the saturation block is placed before the *I*dd* component to operate the DG in optimal fuel efficient zone at change in load, as depicted in Fig. 3.
In this work, a generalized concept is used to calcu late the DG power based on state of the BES. The reference DG power in p u (*P*D*) is computed as,

$$P^*_D = P_{D\min} + k_1\beta \quad (8)$$

Here the value of *β* varies from 0 to 1. The minimum value of *β* is achieved when BES is charged to maximum voltage (*Vbmax*) whereas *β* takes maximum value when BES voltage falls to its minimum value (*Vbmin*). The *β* is of the form a s,

$$\beta = \frac{V_{b\max} - V_b}{k_2} \quad (9)$$

In (8) and (9), *k1* and *k2* represent constant parameters. The value of *k1* is selected such that *P*D* attains its maximum l imit of optimal fuel consumption as *β* tends to unit y. Moreover, the value of *k2* is selected such that the *β* attains unity at *Vbmi n*. In this work, the chosen values of *PDmin*, *PDm ax*, *Vbmax*, *Vbmin*, *k1* and *k2* are mentioned in Appendices.
From (8), the *I*dd* is computed as,

$$I^*_{dd} = \left(\sqrt{2/3}\right) \times \left(\frac{P^*_D \times VA_{DG}}{V_L}\right) \quad (10)$$

where *VL* and *VADG* represent line voltage at PCC and VA rating of DG, which is chosen as a base v alue.
The *I*dw* is computed as,

$$I_{dw}^{*} = \left(\frac{L_m}{L_s}\right) I_{qr} \quad (11)$$

The DG currents (*ida*, *idb* and *idc*) are transformed to *Id* and *Iq* using angle of transformation (*θs*), wh ich is obtained from PLL as shown in Fig.
3. The q-
axis component of LSC current (*I*qg*) is numerical ly same as *Iq* of DG. The *I*dg* and *I*qg* are multip lied with in-
phase and quadrature unit templates, respectively a nd then added together to generate current referenc es (*i*ga*, *i*gb* and *i*gc*). The unit templates are obtained from phase voltages (*va*, *vb* and *vc*), as shown in Fig.
3. Unit templates of in-
phase components are obtained as,

$$u_{ap} = \frac{v_a}{V_m}, u_{bp} = \frac{v_b}{V_m}, u_{cp} = \frac{v_c}{V_m} \quad (12)$$

where, *Vm* denotes the peak of phase voltage at PC C, which is computed as,

$$V_m = \{2(v_a^2 + v_b^2 + v_c^2)/3\}^{1/2} \quad (13)$$

The unit templates of quadrature components, are obtained from in-phase components as,

$$u_{aq} = -\frac{u_{bp}}{\sqrt{3}} + \frac{u_{cp}}{\sqrt{3}}, u_{bq} = \frac{\sqrt{3}u_{ap}}{2} + \frac{u_{bp} - u_{cp}}{2\sqrt{3}}, \quad u_{cq} = -\frac{\sqrt{3}u_{ap}}{2} + \frac{u_{bp} - u_{cp}}{2\sqrt{3}} \quad (14)$$

Finally, the generated reference currents and sense d currents (*iga*, *igb* and *igc*) are applied to PWM c ontroller to produce pulses for LSC, as depicted in Fig. 3.

C. Solar PV Array MPPT Algorithm and Bidirect ional Buck/Boost DC-DC Converter Control

The bidirectional buck or bidirectional boost DC-
DC converter is used to regulate the DC link volta ge by controlling power flow through the BES. By doing
so, the solar MPPT is achieved. In this, a modified perturb and observe (P&O) algorithm is used, whi ch consists of sampling pulse generation (*X*) and su bsequently estimation of reference DC link voltage (*V*dc*) as depicted in Figs. 4-5, respectively. Fig. 4 illustrates various steps involved in the generatio n of sampling pulse '*X*'. Here, the sampling pulse i s a name

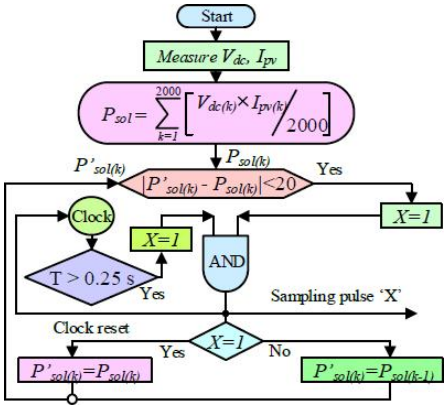

Fig. 5 Sampling pulse generation.

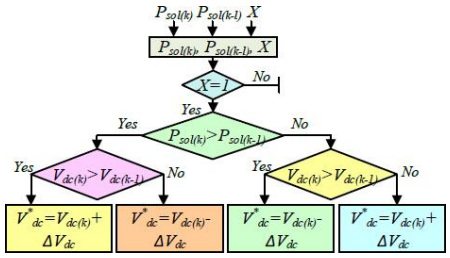

Fig.6. MPPT algorithm of solar PV array.

given to variable '*X*'. It varies between digital bits 0 and 1. In Fig.
4, the first step is to get the information of DC lin k voltage or solar PV voltage (*Vdc*) and solar PV c urrent (*Ipv*) at *k*th instant and computation of insta ntaneous solar power. The second step is the deter mination of running average solar power (*Psol*), w hich performs the same function as filtering. In cas e the absolute difference between the running aver aged power (*Psol*) and previously sampled power (*P'sol*) is less than
20 W combined with minimum time delay of 0.25
s from previous sampling, the control senses that s teady state has arrived. On sensing the steady state, the output of the sampling pulse '*X*' becomes
'1'. The sampling pulse decides the instant of incr emental change in reference DC link voltage (*V*dc*) or solar PV MPPT voltage. The value of *V*dc* is updated only if sampling pulse becomes '1'. This i s clearly evident from Fig.
5 that depicts the modified P&O MPPT algorithm. Once *X* becomes '1', the MPPT algorithm checks for *Psol(k) >Psol(k-1)*. If it is
yes, then it again checks for *Vdc(k) >Vdc(k-1)*. If it is also
yes, then, the new reference DC link voltage beco mes *V*dc = Vdc(k)+ ΔVdc*. Where *ΔVdc* denotes th e small incremental change in DC link voltage. Th e other scenarios are evident from the Fig. 5.
The bidirectional buck/boost DC-
DC converter control, is demonstrated in Fig.

6. The outer proportional-
integral (PI) controller of the bidirectional buck or bidirectional DC-
DC boost converter control, is used to regulate the DC link voltage. Moreover, the output of the outer PI controller is reference battery current (*I*b*), as d epicted in Fig.
6. The inner PI controller is used to track the refer ence battery current. Moreover, the output of the in ner PI controller is the duty ratio (*R*) of the bidirect ional buck/boost DC-DC converter. From Fig.
6, the reference battery current (*I*b*) is obtained as
,

$$I^*_{b(k)} = I^*_{b(k-1)} + K_{pb}(V_{de(k)} - V_{de(k-1)}) + K_{ib}V_{de(k)} \quad (15)$$

Where, error of the DC link voltage at *k*th instant i s . Here *V*dc(k)* and *Vdc(k)* represent the reference DC link voltage and sensed DC link voltage at *k*th instant, respectively. *Kpb* and *Kib* denote the prop ortional and * () () () dek dck dck V V V

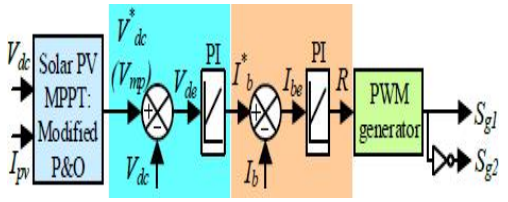

Fig. 7.
Control of bidirectional buck or bidirectional boos t converter.

integral constants of the outer PI controller. Besid es, the duty ratio (*R*) of the bidirectional DC-
DC converter, is computed as,

$$R_{(k)} = R_{(k-1)} + K_{pr}(I_{be(k)} - I_{be(k-1)}) + K_{ir}I_{be(k)} \quad (16)$$

Where, error of the battery current at *k*th instant is $I_{be(k)} = I^*_{b(k)} - I_{b(k)}$.
. Here *I*b(k)* and *Ib(k)* represent the reference batt ery current and sensed battery current at *k*th instant , respectively. The obtained duty ratio (*R*) is appli ed to PWM generator to produce pulses for the swi tches of the bidirectional buck or bidirectional boo st converter.

IV The newly proposed RSC-based scheme with the PI-FUZZY hybrid controller and SCC.

The reference voltage values * Vdqr + for the RSC are computed from the outputs of two PI-FUZZY controllers as described in Fig. 4. The PI-FUZZY controllers can enhance remarkably the in dependence with parametric alterations of the pow er system in generating the reference signals. Also, using the PI with anti-
windup (PI+A) controllers, values of * dqr I + + ca n be obtained suitably from errors between the refe rence and measured signals of the two powers. As aforementioned, the Notch filters are utilized to rej ect the negative sequence components. Nonetheles s, the real response and efficacy of digital Notch fil ters are not entirely flawless; thus the SCC, contain ing the two PI controllers, is designed for combini ng with the Notch filters to can remove thoroughly the negative sequence components of rotor current . In SFOC, with dqr I − − = 0, ψ qr + = 0 and, the rotor current now can be defined by Be sides, the output values of the SCC are * dqr I + − , so it also has function as a current sub-controller for the PI-F and PI–
FUZZY controllers to help regulate the positive se quence components of rotor current. Meanwhile, n ote that negative sequence components of the rotor current will boost the power rating of RSC if they are utilized in stabilizing the two output powers of DFIG. From, the output active power Ps and reacti ve power Qs in stator are computed as follows:

Structure of the PI-FUZZY hybrid controller in

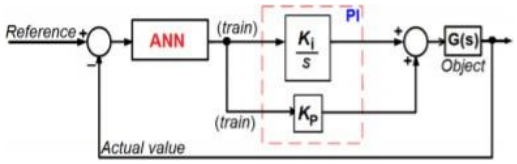

Fig. 8 Design diagram of the PI-FUZZY controller

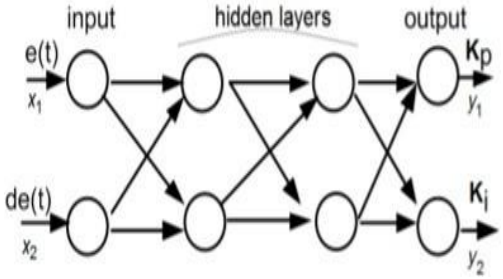

Fig.
9 Detailed structure of the FUZZY with four layer s

The proposed FUZZY in this study utilizi ng RSC control algorithm for performing an offlin e training process to determine suitable values for t he key two coefficients KP and KI of the PI contro ller. As given in Fig.
6, the FUZZY comprises one input layer, two hidd en layers and one output layer. Wherein, the input l ayer has two neurons as the error value e(t) and its derivative value
de(t) of the current as shown in Fig.
4, each hidden layer has two neurons, and the outp ut layer has two neurons as KP and KI . The total

weight value netq and the output value Zq of the j-th neuron in the q-th hidden layer are computed , respectively

$$net_q = \sum v_{qj} x_j \quad (17)$$

$$Z_q = a_h(net_q) = a_h(\sum v_{qj} x_j) \quad (18)$$

Where vqj is the weight gain for the j-th neuron, and is the operational function used for the q-th hidden layer. Then, the total weight value of the i-th neuron in the output layer is expressed, where w iq is the weight gain for the i-th neuron. Lastly, the two coefficients KP and KI are defined by respectively; where a0(.) is the operational function used for the output layer.

$$net_i = \sum w_{iq} Z_q = \sum [w_{iq}.a_h(net_q)] \quad (19)$$

$$K_P = a_0(net_1) = a_0(\sum w_{1q} Z_q) = a_0(\sum [w_{1q}.a_h(net_q)]) \quad (20)$$

$$K_I = a_0(net_2) = a_0(\sum w_{2q} Z_q) = a_0(\sum [w_{2q}.a_h(net_q)]) \quad (21)$$

Where operational functions in hidden and output layers are bipolar sigmoid and linear functions, respectively:

$$a_h(f) = 1/(1 + e^{-f}) \quad (22)$$

$$a_0(f) = f \quad (23)$$

If the number of hidden layers is increased, FUZZY may have a better adaptation. In this study, to evaluate the proposed PI-FUZZY algorithm, two hidden layers can be used such as the simplest structure for implementing in simulation. Where the number of hidden layers is more, the training time becomes longer; which can lead to cause noticeable delay in generating the control signal at output layer. So optimization for the number of hidden layers and time delay will be studied in our future work. As shown in Figs. 5 and 6, the BP algorithm has two main steps in transmitting information between layers as follows. Firstly, the input data x(k) is transmitted forward to generate the value y(k) at the output. Then, the error value E(k) between the reference value in the data set d(k) and the above output value y(k) is transmitted back to the previous layer to update fittingly the weight gains vqj. The data set utilized for the offline training process is S{x(k),d(k)}, and the goal of this training process is to minimize the error E(k+1) as given. Normally, the offline training process in FUZZY is performed sometimes with several data sets to achieve a good result as desired.

$$E(k+1) = E(k) + 0.5\sum [d_i(k) - y_i(k)] \rightarrow \mathbf{min} \quad (24)$$

IV Simulation Results for the New DFIG Scheme.

The microgrid based on wind turbine driven DFIG, DG and solar PV array with BES, is simulated using MATLAB. Various signals used to analyze the system performance, are rms value of phase voltage (*Vr*), system frequency (*fL*), DFIG rotor speed (*ωr*), DG power (*PD*), wind power from stator (*Pw*), solar PV power (*Psol*), load power (*PL*), LSC power (*PLSC*), DC link voltage (*Vdc*), battery current (*Ib*), battery voltage (*Vb*), wind speed (*Vw*), insolation (*G*), rotor power coefficient (*Cp*), a-phase stator current (*isa*), rotor currents (*irabc*), a-phase DG current (*ida*), a-phase PCC voltage (*vLa*), stator currents (*isabc*), DG currents (*idabc*), load currents (*iLa*, *iLb* and *iLc*), neutral current (*iLn*) and LSC currents (*icabc*). The parameters used for the simulation are mentioned in Appendices.

A. Performance of Bidirectional Buck/Boost DC-DC Converter at Change in Load

The performance of bidirectional buck or bidirectional boost DC-DC converter at change in the load, is depicted in Figs. 7 (a-b). The wind speed and insolation are kept at 7 m/s and 700 W/m2, respectively. Initially a 3-phase balanced load of 2.5 kW is connected at PCC. The DG is delivering 4.84 kW (shown in Fig. 7 (b)), which corresponds to the battery bank voltage of 125 V. Moreover, the DFIG and solar PV array powers are 2.013 kW and 4.122 kW, respectively as depicted in Fig. 7 (b). Since the total generation is more than the local demand, the remaining power goes to BES through a bidirectional buck/boost DC-DC converter as shown in Fig. 7 (a). At t = 3 s, an additional load of 2 kW is connected and again it is disconnected at t = 5.5

s. During this period, it is observed that the power generation from all sources, remains unchanged a nd the increased load power is met by the BES thr ough LSC. There is a minor sag and swell of DC li nk voltage, however, the solar MPPT is unaffected as seen from *Psol* waveform. Moreover, the system voltage and frequency are maintained constant, as depicted in Fig. 7 (b).

B. System Performance at Variable Wind Speeds

The performance of the system at variable wind sp eeds are depicted in Figs. 8 (a-c). In this, a 3-phase load of
4 kW is connected at PCC and the insolation is ke pt at 700 W/m2. The DG delivers power of
5.67 kW based
on the state of the BES, as depicted in Fig.
8 (b). The pattern of wind speed variation is depic ted in Fig.
8 (a). It is observed that the controller regulates th e DFIG rotor speed as per wind MPPT algorithm, as depicted in Fig.
8 (a). Moreover, it is observed that the DC link vo ltage is regulated. The system dynamic response d uring the transition of DFIG speed from super sync hronous to sub synchronous speed region, is depict ed in Fig.
8 (c). It is observed that wind MPPT is obtained d uring the variation of wind speed. Moreover, the fr equency rotor currents, is changed according to the speed of operation of DFIG.

C. System Performance at Variable Insolation

The performance of the system at varying solar rad iation, is depicted in Figs. 9 (a-b). In this, the wind speed is kept constant at
7 m/s. Moreover, the DG delivers
4.2 kW power based
on the battery voltage, as depicted in Fig.
9 (b). In this, a 3-phase linear balanced load of nearly
4 kW is connected at PCC. The insolation of solar PV array is varied from 700 W/m2 to 800 W/m2 at t = 3 s and again it is reduced to 600 W/m2 at t = 5.5 s, as depicted in Fig. 9 (a). The DC link voltage is regulated by the bidi rectional DC-DC converter control for achieving the solar MPPT . Moreover, the solar MPPT is manifested by the *P sol* waveform, as depicted in Fig. 9 (a).

D. System Performance at Unbalanced Nonlinear Load

The dynamic performance of the system at unbalan ced nonlinear load, is depicted in Fig.
10. Initially, a balanced load of
6.7 kW is connected at PCC. It includes a linear lo ad of
0.5 kW and remaining be the nonlinear load, conn ected on each phase. At t = 2.6 s, a-phase of the load is disconnected and subsequently phase-b, is also disconnected at t = 2.8 s, as depicted in Fig.
10. However, both voltages and currents of DFIG and DG, are maintained balanced and follow the I EEE
519 standard. The LSC helps in unbalance and har monics compensation of the connected load at PC C. The LSC currents and neutral current, are also s hown in Fig.
10. Moreover, the variation of power at unbalance d nonlinear load, is depicted in Fig. 11. Fig. 11 demonstrates waveforms of *Vr*, *Vdc*, *Ib*, *Psol*, *Pw*, *PD*, *PL* and *PLSC*. From these results, it is obs erved that the DC link voltage is regulated and mor eover, solar PV and wind MPPT operation is unaff ected. The decrease in load power goes to BES thr ough LSC, which is evident from *Ib*, *PL* and *PLSC* waveforms. Moreover, *Vr* is maintained at constan t value.

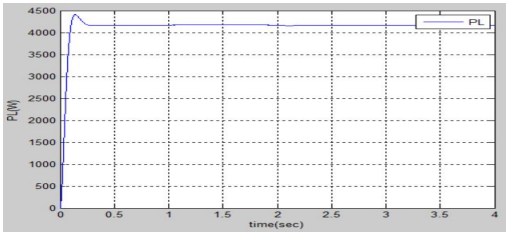

(a)

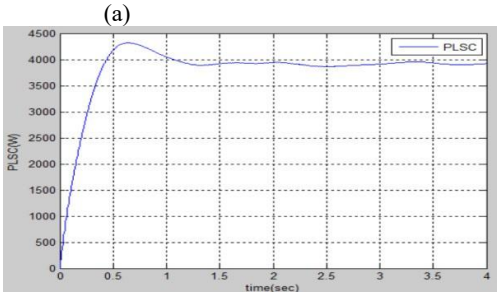

(b)

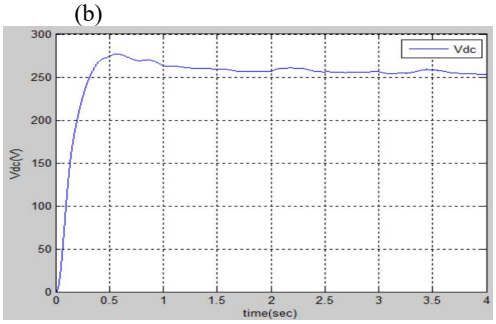

(c)

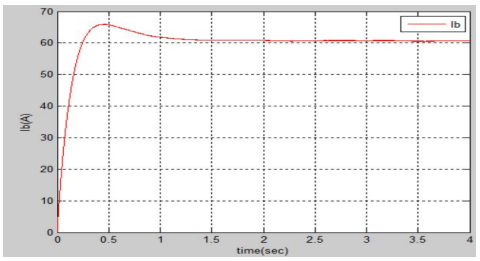

(d)

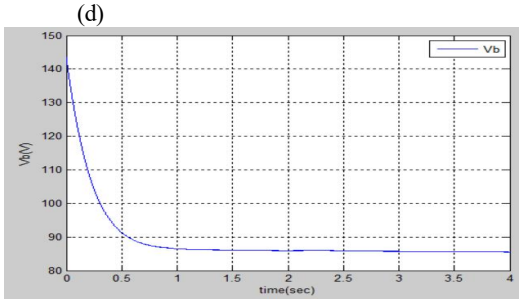

(e)

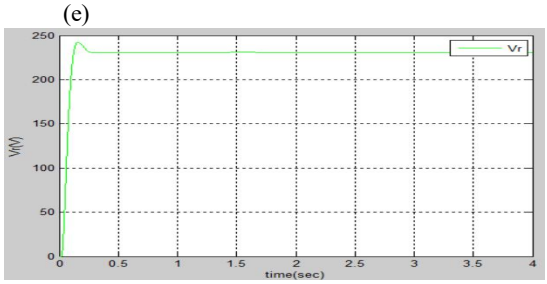

(f)

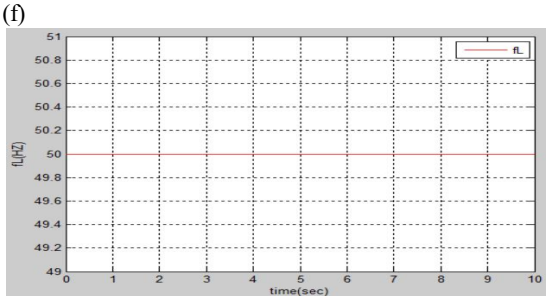

(g)

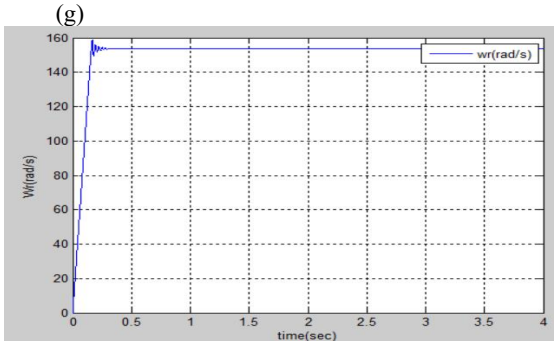

(h)

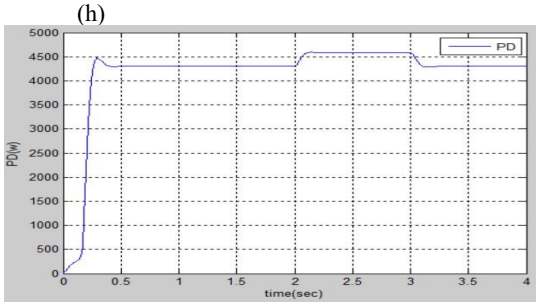

(i)

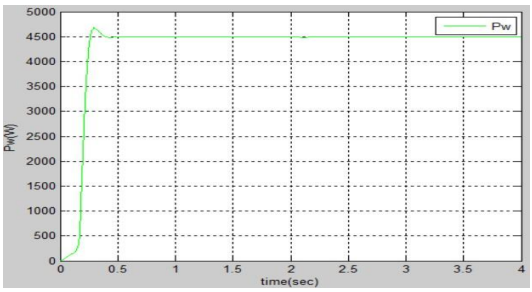

(j)

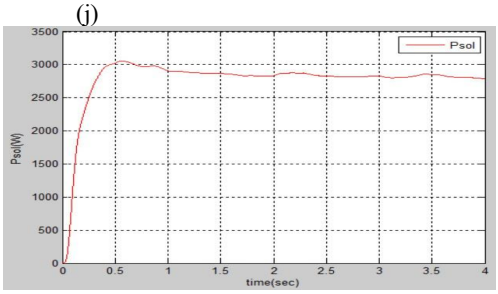

(k)

Fig. 10. (a-b) Performance of bidirectional buck/boost converter at change in load (a) *PL*, *PLSC*, *Vdc*, *Ib* and *Vb* (b) *Vr*, *fL*, *ωr*, *PD*, *Pw* and *Psol*.

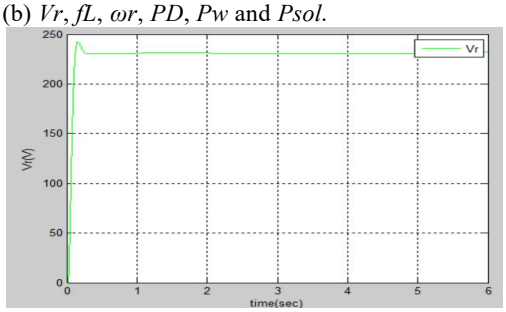

(a)

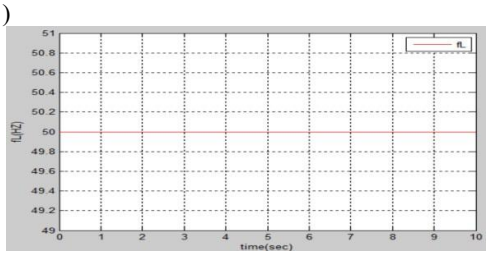

(b)

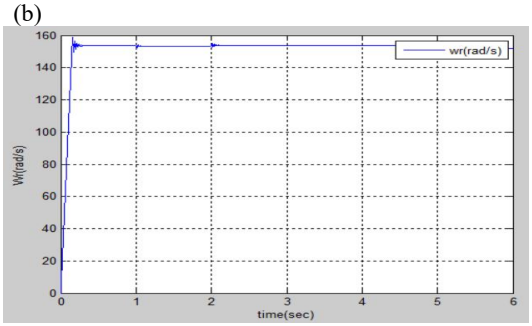

(c)

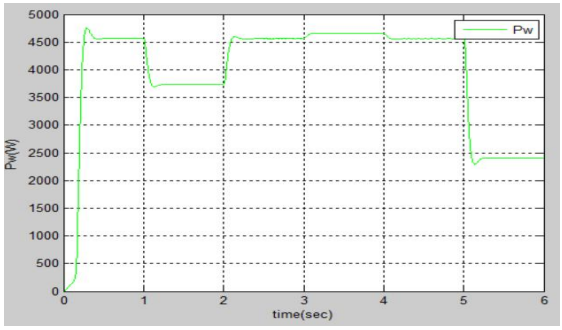
Pw
Pw(W)
time(sec)

(d)

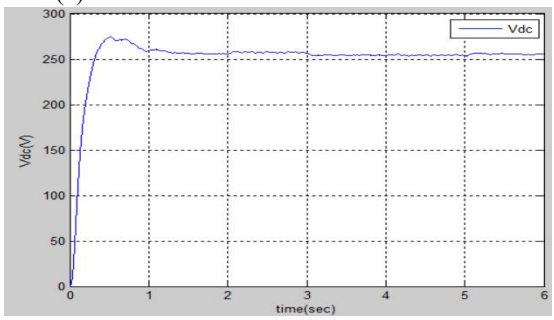
Vdc
Vdc(V)
time(sec)

(e)

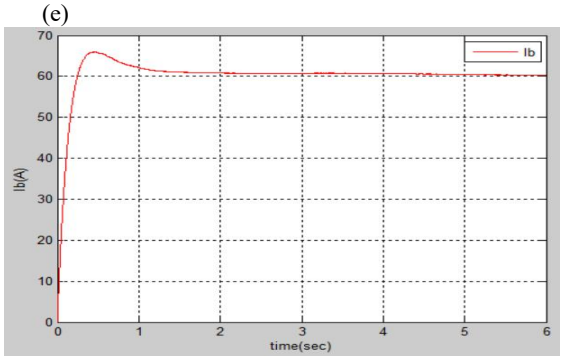
Ib
Ib(A)
time(sec)

(f)

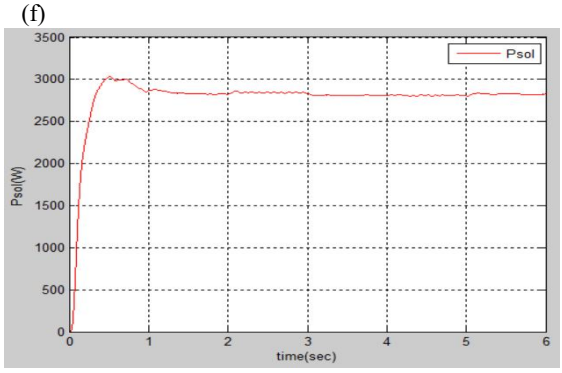
Psol
Psol(W)
time(sec)

(g)

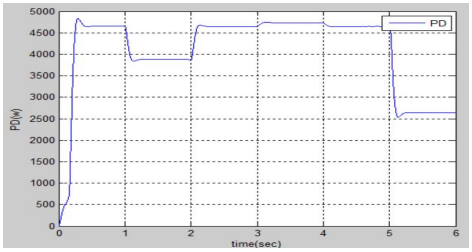
PD
P0(w)
time(sec)

(h)

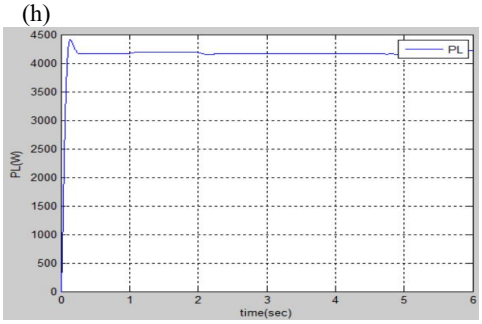
PL
PL(W)
time(sec)

(i)

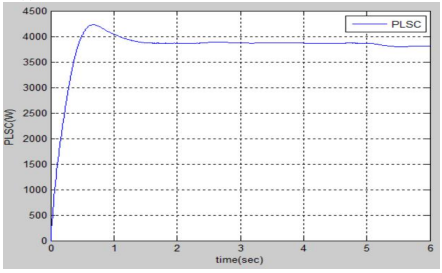
PLSC
PLSC(W)
time(sec)

(j)

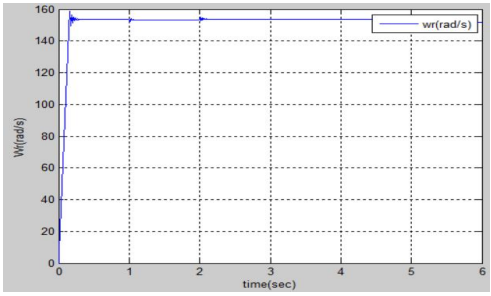
wr(rad/s)
Wr(rad/s)
time(sec)

(k)

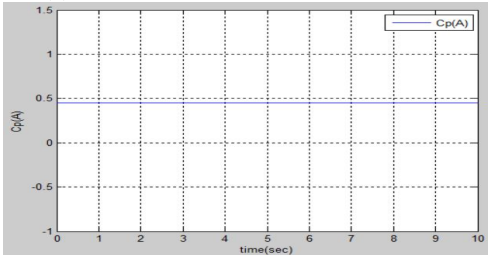
Cp(A)
Cp(A)
time(sec)

(L)

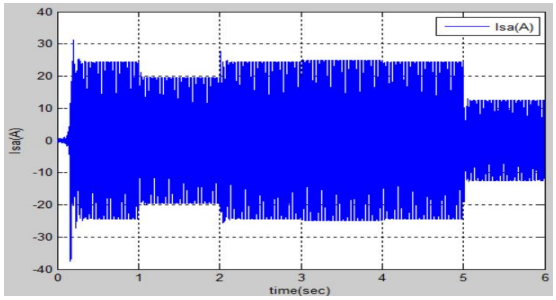

(m)

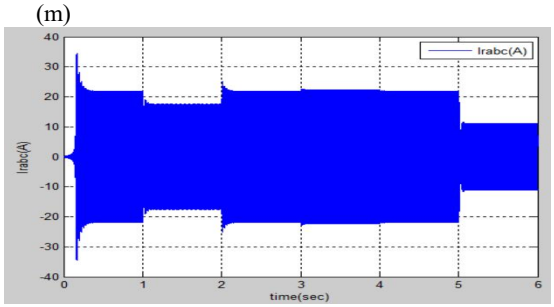

(n)

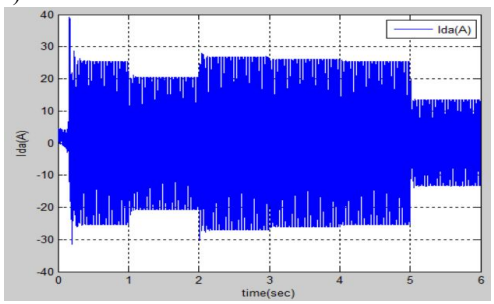

(o)

Fig. 11. System performance at variable wind speed (a) *Vr*, *fL*, *Vw*, *ωr* and *Pw* (b) *Vdc*, *Ib*, *Psol*, *PD*, *PL* and *PLSC*. (c) system performance during changeo ver of DFIG speed from supersynchronous to subs ynchronous speed region: *Vw*, *ωr*, *Cp*, *isa*, *irabc* an d *ida*.

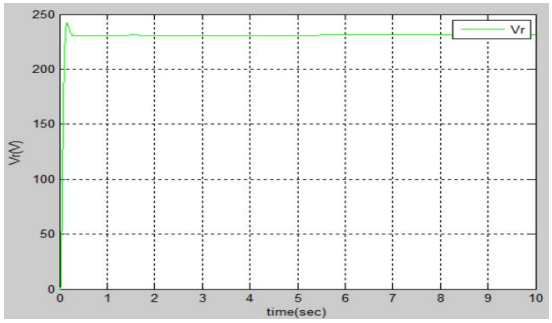

(a)

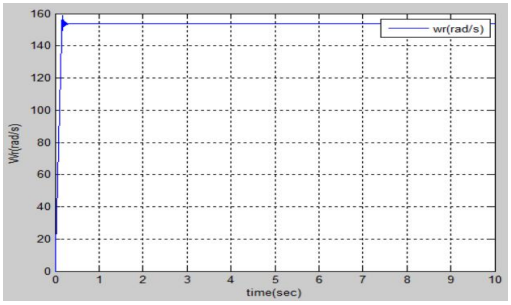

(b)

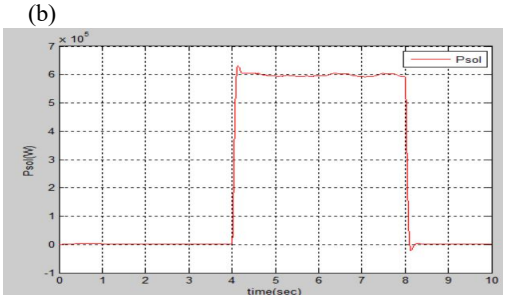

(c)

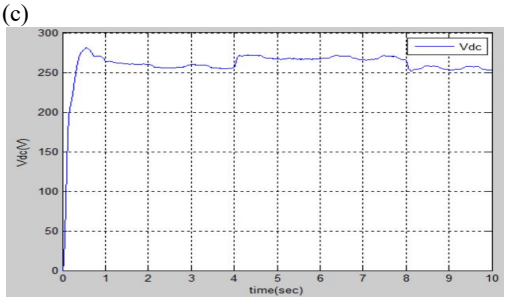

(d)

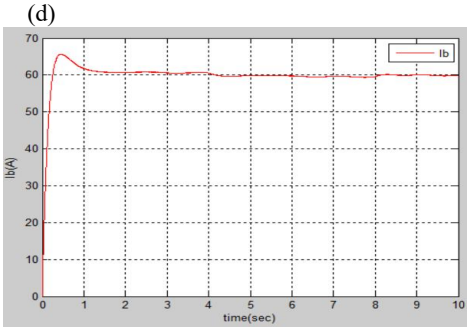

(e)

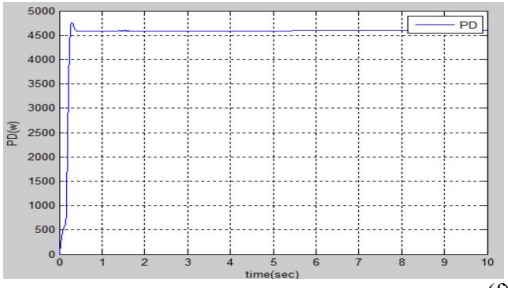

(f)

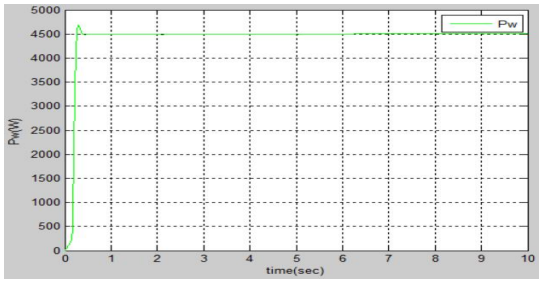

(g)

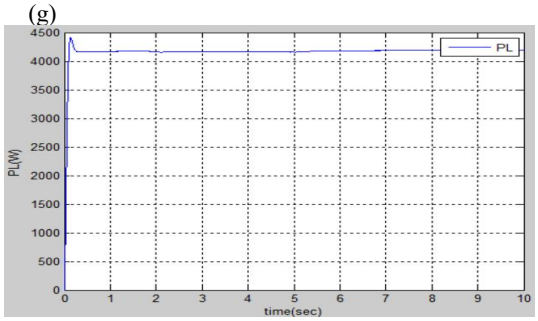

(h)

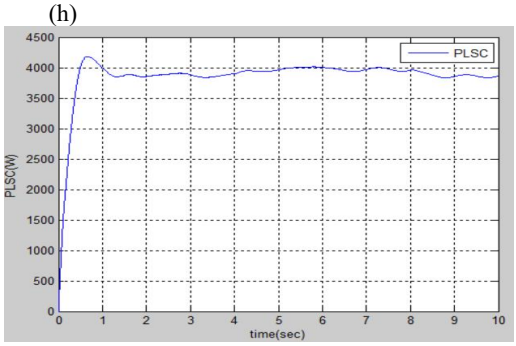

(i)

Fig.12. System performance at variable insolation (a) *Vr*, *ωr*, *G*, *Psol* and *Vdc* (b) *Ib*, *PD*, *Pw*, *PL* and *PLSC*.

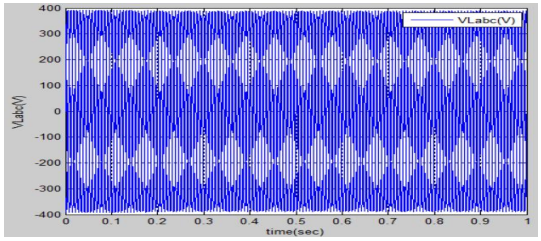

(a)

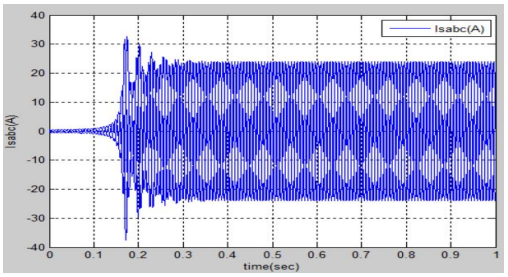

(b)

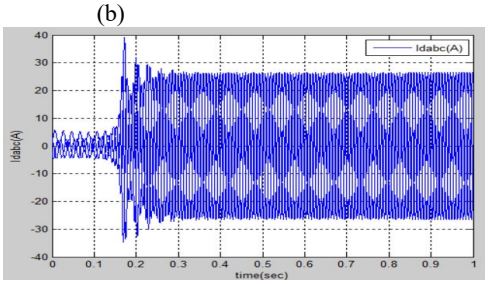

(c)

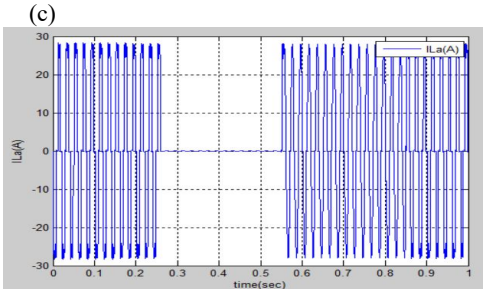

(d)

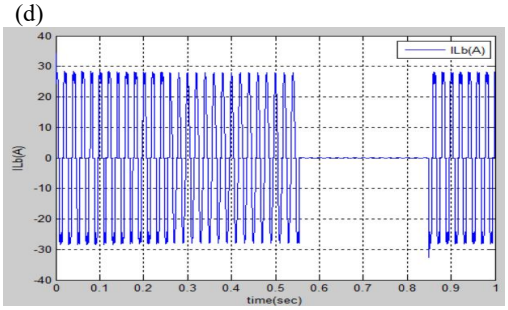

(e)

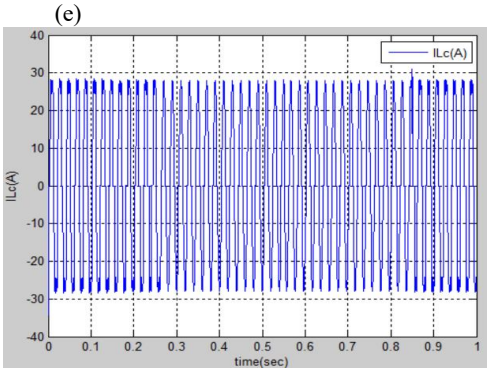

(f)

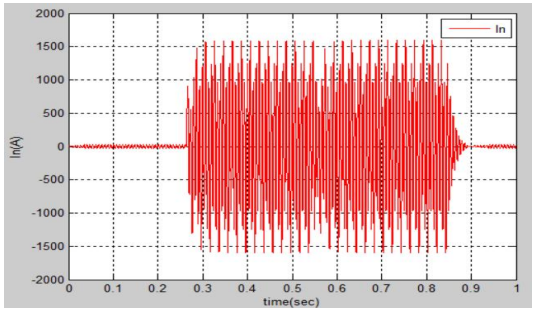
In
In(A)
time(sec)

(g)

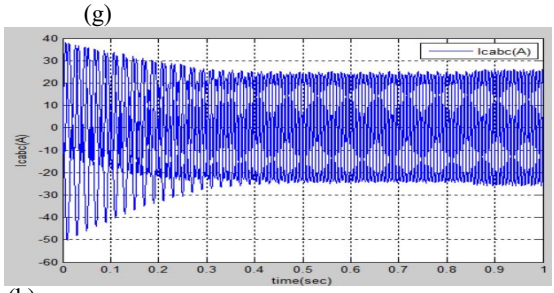
Icabc(A)
Icabc(A)
time(sec)

(h)

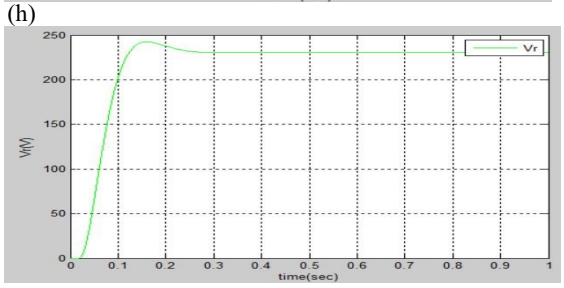
Vr
Vr(V)
time(sec)

(i)

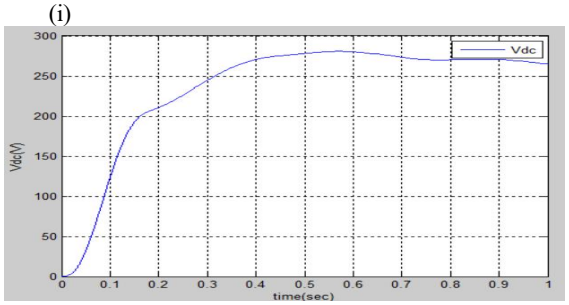
Vdc
Vdc(V)
time(sec)

(j)

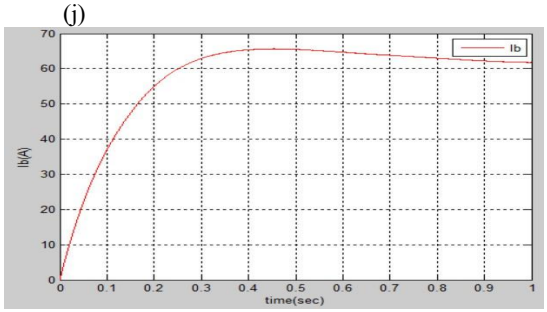
Ib
Ib(A)
time(sec)

(k)

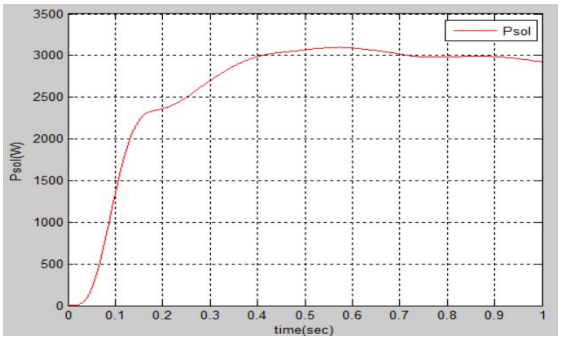
Psol
Psol(W)
time(sec)

(L)

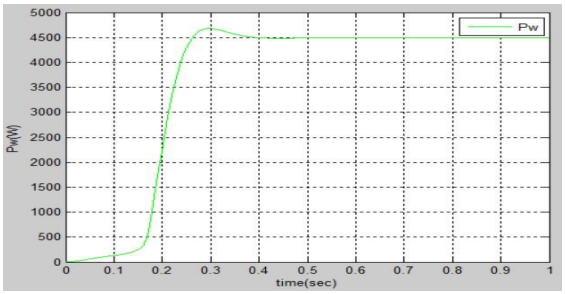
Pw
Pw(W)
time(sec)

(m)

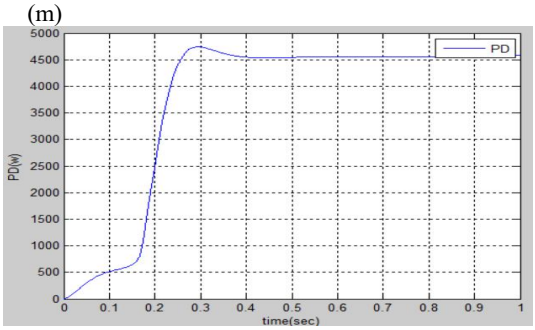
PD
PD(w)
time(sec)

(n)

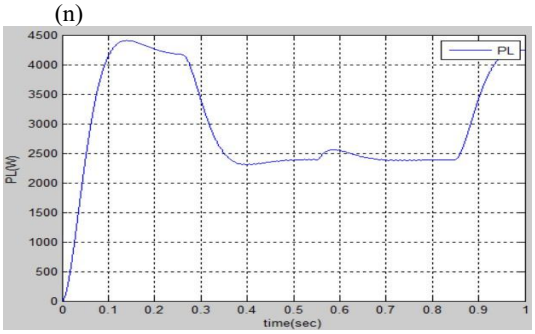
PL
PL(W)
time(sec)

(m)

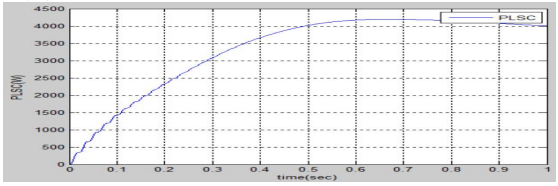
PLSC
PLSC(W)
time(sec)

(o

)

Fig.13. System performance at nonlinear unbalanced load: *Vr*, *Vdc*, *Ib*, *Psol*, *Pw*, *PD*, *PL* and *PLSC*.

V. CONCLUSION

The proposed system has promising scope for islands, which are totally dependent on the diesel-based generation. The load regulation capability of the diesel generator to operate in Efficient fuel zone reduces specific fuel consumption. The MPPT feature of proposed system in control, helps in maximizing generation and further helps to reduce the cost of the energy. The system is also able to maintain phase currents balanced as well as and current harmonics within an acceptable limit for all types of loads. The effectiveness of the system is demonstrated using simulated and test results and it is found that the power quality is within acceptable limit under all practical scenarios.

REFERENCES

[1] J. Knudsen, J. D. Bendtsen, P. Andersen, K. K. Madsen, and C. H. Sterregaard, "Supervisory control implementation on diesel-driven generator sets," *IEEE Trans. Ind. Electron.*, vol. 65, no. 12, pp. 9698-9705, Dec. 2018.

[2] J. Jo, H. An, and H. Cha, "Stability improvement of current control by voltage feedforward considering a large synchronous inductance of a diesel generator," *IEEE Trans. Ind. Applicat.*, vol. 54, no. 5, pp. 5134-5142, Sept.-Oct. 2018.

[3] Y. Zhang, A. M. Melin, S. M. Djouadi, M. M. Olama and K. Tomsovic, "Provision for guaranteed inertial response in diesel-wind systems via model reference control," *IEEE Trans. Power Systems*, vol. 33, no. 6, pp. 6557-6568, Nov. 2018.

[4] N. Nguyen-Hong, H. Nguyen-Duc, and Y. Nakanishi, "Optimal sizing of energy storage devices in isolated wind-diesel systems considering load growth uncertainty," *IEEE Trans. Ind. Applicat.*, vol. 54, no. 3, pp. 1983-1991, May-June 2018.

[5] W. Li, P. Chao, X. Liang, J. Ma, D. Xu, and X. Jin, "A practical equivalent method for DFIG wind farms," *IEEE Trans. Sustain. Energy*, vol. 9, no. 2, pp. 610-620, April 2018.

[6] T. Adefarati, R. C. Bansal, and J. John Justo, " Techno-economic analysis of a PV–wind–battery– diesel standalone power system in a remote area," *The Journal of Engineering*, vol. 2017, no. 13, pp. 740-744, 2017.

[7] C. Wu and H. Nian, "Stator harmonic currents suppression for DFIG based on feed-forward regulator under distorted grid voltage," *IEEE Trans. Power Electron*., vol. 33, no. 2, pp. 1211-1224, Feb. 2018.

[8] N. K. Swami Naidu and B. Singh, "Experimental implementation of doubly fed induction generator-based standalone wind energy conversion system," *IEEE Trans. Ind. Applicat.*, vol. 52, no. 4, pp. 3332-3339, July-Aug. 2016.

[9] D. Sun, X. Wang, H. Nian, and Z. Q. Zhu, "A sliding-mode direct power control strategy for DFIG under both balanced and unbalanced grid conditions using extended active power," *IEEE Trans. Power Electron*., vol. 33, no. 2, pp. 1313-1322, Feb. 2018.

[10] Ju Liu, Wei Yao, Jinyu Wen, Jiakun Fang, Lin Jiang, Haibo He, and Shijie Cheng, "Impact of power grid strength and PLL parameters on stability of grid-connected DFIG wind farm," *IEEE Trans. Sustain. Energy*, vol. 11, no. 1, pp. 545-557, Jan. 2020.

[11] A. Thakallapelli, S. Kamalasadan, K. M. Muttaqi, and M. T. Hagh, "A synchronization control technique for soft connection of doubly fed induction generator based wind turbines to the power grids, " *IEEE Trans. Ind. Applicat.*, vol. 55, no. 5, pp. 5277-5288, Sept.-Oct. 2019.

[12] P. Shah, I. Hussain, and B. Singh, "Single-stage SECS interfaced with grid using ISOGI-FLL-based control algorithm," *IEEE Trans. Ind. Applicat.*, vol. 55, no. 1, pp. 701-711, Jan.-Feb. 2019.

[13] A. K. Singh, I. Hussain, and B. Singh, "Double-stage three-phase grid-integrated solar PV system with fast zero attracting normalized least mean fourth based adaptive control," *IEEE Trans. Ind. Electron.*, vol. 65 no. 5, pp. 3921-3931, May 2018.

[14] M. J. Morshed and A. Fekih, "A novel fault ride through scheme for hybrid wind/PV power generation systems," *IEEE Trans. Sustainable Energy*, Early Access.

[15] S. K. Tiwari, B. Singh, and P. K. Goel, "Design and control of autonomous wind–solar system with DFIG feeding 3-phase 4-wire loads," *IEEE Trans. Ind. Applicat.*, vol. 54, no. 2, pp. 1119-1127, March-April 2018.

[16] Y. Zhang, J. Wang, A. Berizzi, and X. Cao, " Life cycle plFuzzying of battery energy storage system in off-grid wind–solar–diesel microgrid," *IET Gener., Trans. & Distr.*, vol. 12, no. 20, pp. 4451-4461, Nov. 2018.

[17] S. K. Tiwari, B. Singh, and P. K. Goel, "Control of wind–diesel hybrid system with BESS for optimal operation," *IEEE Trans. Ind. Applicat.*, vol. 55, no. 2, pp. 1863-1872, March-April 2019.

[18] K. Venkatraman, B. Dastagiri Reddy, M. P. Selvan, S. Moorthi, N. Kumaresan, and N. A. Gounden, "Online condition monitoring and power management system for standalone micro-grid using FPGAs," *IET Gener., Trans. & Distr.*, vol. 10, no. 15, pp. 3875-3884, Nov. 2016.

[19] S. Puchalapalli and B. Singh, "A single input variable FLC for DFIG-based WPGS in standalone mode," *IEEE Trans. Sustainable Energy*, vol. 11, no. 2, pp. 595-607, April 2020.

[20] J. Hussain and M. K. Mishra, “Adaptive maxi mum power point tracking control algorithm for wi nd energy conversion systems,” *IEEE Trans. Ener gy Convers.*, vol. 31, no. 2, pp. 697-705, June 2016.
[21] S. Puchalapalli, S. K. Tiwari, B. Singh, and P. K. Goel, “A microgrid based on wind driven DFIG, DG and solar PV array for optimal fuel consumption,” in *8th IEEE Power India International Conference (PIICON)*, Kurukshetra, India, 2018, pp. 1-6.

PandlaVyshnaviwas born in AP, India. Currently she is studying her M.Tech in Electrical &Electronics Engineering from Sri PadamavatiMahila University, Tirupathi ,Andhrapradesh.

D.Himabindu iscurrently pursuing ph.D.in the department of EEE JNTUA university,Ananthapur and also working as an assistant professor-department of EEE in SOET ,SPMVV,TirupatiAP,India .Her-research-interests include power electronics ,electrical-machines,&Modelling&Analysis of AC drives.she is a life member of ‘ISTE’.